Biosensors and Bioelectronics 31 (2012) 244–250

Contents lists available at SciVerse ScienceDirect

Biosensors and Bioelectronics

journal homepage: www.elsevier.com/locate/bios

Indirect electrocatalytic determination of choline by monitoring hydrogen peroxide at the choline oxidase-prussian blue modified iron phosphate nanostructures

Hui Zhang[a,*], Yajing Yin[a,b], Ping Wu[a], Chenxin Cai[a,*]

[a] Jiangsu Key Laboratory of New Power Batteries, Jiangsu Key Laboratory of Biofunctional Materials, Laboratory of Electrochemistry, College of Chemistry and Materials Science, Nanjing Normal University, Nanjing 210097, PR China
[b] Editorial Department of Journal of Jiangsu Institute of Education, Jiangsu Institute of Education, Nanjing 210013, PR China

ARTICLE INFO

Article history:
Received 30 September 2011
Accepted 14 October 2011
Available online 9 November 2011

Keywords:
Iron phosphate
Prussian blue
Choline oxidase
Choline biosensor
Electrochemical method

ABSTRACT

Choline, as a marker of cholinergic activity in brain tissue, is very important in biological and clinical analysis, especially in the clinical detection of the neurodegenerative disorders disease. This work presents an electrochemical approach for the detection of choline based on prussian blue modified iron phosphate nanostructures (PB–$FePO_4$). The obtained nanostructures showed a good catalysis toward the electroreduction of H_2O_2, and an amperometric choline biosensor was developed by immobilizing choline oxidase on the PB–$FePO_4$ nanostructures. The biosensor exhibited a rapid response (ca. 2 s), low detection limit ($0.4 \pm 0.05\,\mu M$), wide linear range (2 μM to 3.2 mM), high sensitivity (~$75.2\,\mu A\,mM^{-1}\,cm^{-2}$), as well as good stability and repeatability. In addition, the common interfering species, such as ascorbic acid, uric acid and 4-acetamidophenol did not cause obvious interference due to the low detection potential (−0.05 V versus saturated calomel electrode). This nanostructure could be used as a promise platform for the construction of other oxidase-based biosensors.

1. Introduction

Choline, as an essential physiological component of the cerebral spinal fluid, distribute in peripheral and central nervous systems of mammals. It is often used as a marker of cholinergic activity in the brain tissue, especially in the field of clinic detection of the neurodegenerative disorders disease, such as Parkinson's and Alzheimer's diseases (Jenny et al., 2002; Margrit et al., 2003; Rinne et al., 1991). Therefore, the quantitative determination of choline is very important in biological and clinical analysis (Campanella et al., 1985, 1987; Zhang et al., 2010).

To date, various techniques have been developed for choline determination, including electrochemical method (Bai et al., 2007, 2008; Qin et al., 2009, 2010; Razola et al., 2003; Ren et al., 2009; Shi et al., 2006; Shimomura et al., 2009; Wang et al., 2006; Yang et al., 2004), capillary zone electrophoresis (Carter and Trenerry, 1996; Zhang et al., 2004), HPLC (Ikarashi and Maruyama, 1993), fluorescence method (Fleming and Gadsden, 1987; Sanz-Vicente et al., 2009), and so on. Among those methods, the electrochemical approach has attracted significant attention because of its high sensitivity, low cost, rapid response, compatibility for miniaturization, and low manpower requirements. The electrochemical approach for determination of choline is often based on the enzyme reaction where choline oxidase (ChOx) catalyzes the oxidation of choline to betaine aldehyde, and producing H_2O_2 simultaneously. Thus, quantification of choline could be achieved by measuring the amount of enzymatically generated H_2O_2 by electrochemical method (Bai et al., 2007, 2008; Qin et al., 2009, 2010; Razola et al., 2003; Ren et al., 2009; Shi et al., 2006; Shimomura et al., 2009; Wang et al., 2006; Yang et al., 2004). Generally, the determination of H_2O_2 is based on the direct oxidation of H_2O_2. However, the oxidation of H_2O_2 usually requires a relatively high positive potential (usually over +0.6 V versus saturated calomel electrode) (Qin et al., 2009; Shi et al., 2006; Shimomura et al., 2009). Many other electroactive species coexisting in the biological fluids could also be oxidized at such a high potential, and their electrochemical signals thus severely affect the selectivity of the assay. Therefore, interference elimination represents a main task to be solved for electrochemical method.

The interference can be partially overcome by coating the electrode with a polymer membrane, which is impermeable to interfering species (Qin et al., 2009). However, coating polymer leads to lower signals and longer response time due to the additional diffusion barrier. Another method to overcome the interference is to monitor the generated H_2O_2 at a relatively negative

* Corresponding authors. Tel.: +86 25 85891780; fax: +86 25 85891767.
E-mail addresses: zhangh@njnu.edu.cn, zhanghuihsd@163.com (H. Zhang), cxcai@njnu.edu.cn (C. Cai).

0956-5663/$ – see front matter © 2011 Elsevier B.V. All rights reserved.
doi:10.1016/j.bios.2011.10.026

potential. There are two low-potential transducers for H_2O_2 reduction: peroxidase (Razola et al., 2003; Wang et al., 2006; Yang et al., 2004; Zhang et al., 2010) and electro-transfer mediator such as metal hexacyanoferrate (Shi et al., 2006; G. Zhao et al., 2005; W. Zhao et al., 2005). However, despite the low detection limits achieved, the use of the peroxidase obviously deteriorates transducer properties for its poor stability and high cost (Karyakin et al., 2004). Prussian blue (PB), as a prototype of metal hexacyanoferrate with the formula $Fe_4^{III}[Fe^{II}(CN)_6]_3$ has been widely used as the electron-transfer mediator in the electrochemical biosensor because of the excellent electrocatalytic properties (Karyakin et al., 2000, 2002, 2004; Katz and Willner, 2004; G. Zhao et al., 2005; W. Zhao et al., 2005). Since the H_2O_2 generated from enzymatic reaction can be catalyzed by PB in a negative potential range, the interference from the coexisting substances can be avoided or greatly reduced.

Due to their high surface area and good adsorption ability, many nanomaterials are used for the immobilization of PB nanoparticles to improve the sensor's stability and activity (Ding et al., 2008; Qiu et al., 2008; Wang and Huang, 2011). As an important class of inorganic nanomaterials, iron phosphate ($FePO_4$) nanomaterials have attracted considerable research attention for their low cost, environmental friendliness, and promising electrochemical properties (Okawa et al., 2008; Ramana et al., 2009). In addition, they are good catalysts for the oxidation of glycolic acid and selective oxidation of methane (Mamoru, 2003; Ren et al., 2003). The high specific surface areas and good biocompatibility enable the nanostructures suitable for protein loading and biosensor fabrication (Yin et al., 2010). In this work, we presented a simple approach to synthesize PB nanoparticles modified $FePO_4$ nanostructures (denoted as PB–$FePO_4$) and apply them to fabricate the choline biosensors. Various parameters influencing biosensor performance, including the solution pH, performance temperature and detection potential, were investigated in detail and optimized. Our results demonstrated that the PB–$FePO_4$ nanostructures have potential applications in constructing highly sensitive, stable, and fast response choline biosensor. In addition, due to the low operating potential, the biosensor greatly eliminates the influence of interfering species such as ascorbic acid, uric acid and 4-acetamidophenol.

2. Experimental

2.1. Chemicals

Choline oxidase (ChOx, from alcaligenes species, 12 units/mg) was purchased from Sigma. Cetyltrimethylammonium bromide (CTAB), ammonium ferrous sulfate hexahydrate ($(NH_4)_2Fe(SO_4)_2{\cdot}6H_2O$), phosphoric acid ($H_3PO_4$), hydrochloric acid (HCl), ferric(III) chloride ($FeCl_3$), potassium ferrocyanide ($K_4[Fe(CN)_6]$), urea, ascorbic acid (AA), uric acid (UA) and sodium hydroxide (NaOH) were purchased from Shanghai Chemicals Regent Co. Ltd. (Shanghai, China). Poly(diallyldimethylammonium chloride) (PDDA, MW 200,000–350,000), choline chloride and iron(III) phosphate dihydrate ($FePO_4{\cdot}2H_2O$) were obtained from Aldrich. Solution of H_2O_2 was freshly diluted from the 30% solution and its concentration was determined using a standard solution of $KMnO_4$. 0.1 M phosphate buffer solution (PBS, pH 8.0), which made from K_2HPO_4 and NaH_2PO_4 was employed as the supporting electrolyte. Other chemicals were analytical grade. All chemicals used without further purification and all solutions were prepared with double distilled water.

2.2. Synthesis of $FePO_4$, PB–$FePO_4$ and PB nanostructures

The $FePO_4$ nanostructures were prepared according to the previous report (Yin et al., 2010). Briefly, urea (1.2 g) and CTAB (0.1 g) were dissolved in 40 mL $(NH_4)_2Fe(SO_4)_2{\cdot}6H_2O$ (0.1 mM) solution, followed by the addition of 6.83 μL H_3PO_4. The mixture was vigorously stirred until a homogeneous solution was formed. Then the mixture was transferred into a round-bottom flask, and placed in a homemade microwave refluxing synthesis system at 200 W for 6 min. The resulting products were collected by centrifugation, washed sequentially with double distilled water for three times, and dried in air at room temperature.

PB–$FePO_4$ nanostructures were prepared as follows: 0.18 g $FePO_4$ nanostructures were dispersed into 20.0 mL water and pH was adjusted to 2.0–3.0 with 0.1 M HCl. Then 0.10 M $K_4Fe(CN)_6$ (5.0 mL) was added dropwise to the flask under stirring, and the resultant mixture was stirred for 1 h. The obtained particles were then collected by centrifugation, washed sequentially with double-distilled water and ethanol for several times, and dried under vacuum at room temperature.

For comparison, PB nanostructures were prepared by the reaction of $FeCl_3$ and $K_4Fe(CN)_6$. In brief, 5.0 mL of 0.20 M $K_4Fe(CN)_6$ was dropwisely added to 5.0 mL $FeCl_3$ solution (0.14 g $FeCl_3$ dissolved in 5.0 mL of 0.1 M HCl solution), and the resultant mixture was stirred for 1 h. The obtained products were then collected by centrifugation, washed sequentially with double-distilled water and ethanol for several times, and dried under vacuum at room temperature.

2.3. Immobilization of ChOx and fabrication of ChOx–PDDA–PB–$FePO_4$/GC electrode

For the immobilization of the ChOx, the glassy carbon (GC, 3 mm in diameter, CH Instruments) electrode was polished sequentially with metallographic abrasive paper and slurries of 0.3 and 0.05 μm alumina to create a mirror finish; the electrode was then sonicated with absolute ethanol and double-distilled water for about 1 min, respectively, and dried at ambient temperature.

5 μL suspension of PB–$FePO_4$ (5 mg/mL), which was prepared by sonicating the PB–$FePO_4$ nanostructures in water for 1 min, was drop-cast onto the surface of the electrode with a microsyringe. The solvent evaporated at room temperature before use (denoted as the PB–$FePO_4$/GC electrode). Then the PB–$FePO_4$/GC electrode was immersed in PDDA solution (3 mg/mL) for 40 min, to deposit the polycationic PDDA layer (denoted as the PDDA–PB–$FePO_4$/GC electrode). After being rinsed with water to remove the weakly adsorbed PDDA, the ChOx was immobilized by incubating the PDDA–PB–$FePO_4$/GC electrode in ChOx solution (5 mg/mL in pH 8.0 PBS) for 6 h. Since ChOx (isoelectric point (p*I*) is ~4.5) (Qin et al., 2009) is negatively charged in pH 8.0 PBS, it could spontaneously adsorbed on the surface of the positive charge PDDA–PB–$FePO_4$ via electrostatic interactions. The resulting electrode (denoted as the ChOx–PDDA–PB–$FePO_4$/GC electrode) was rinsed with water thoroughly to remove those loosely adsorbed ChOx molecules. The electrode was stored at 4 °C when not in use. The ChOx–$FePO_4$/GC and ChOx–PDDA–PB/GC electrodes were fabricated using the similar procedures. The ChOx/GC electrode was prepared by dropping 5 μL ChOx solution (5 mg/mL in pH 8.0 PBS) onto the surface of the GC electrode with a microsyringe, the solvent was allowed to evaporate at 4 °C before use.

2.4. Apparatus and procedures

A homemade microwave synthesis system with a maximum output power of 800 W was used for the preparation of the $FePO_4$ nanostructures. Transmission electron microscopic (TEM) images were obtained on a JEOL-2010 microscope with an accelerating voltage of 200 kV. X-ray diffraction (XRD) patterns were recorded on a Rigaku/Max-3A X-ray diffractometer with Cu Kα radiation (λ = 0.15418 nm). The Fourier transform infrared (FT-IR) spectrum was recorded on a Nexus 670 FT-IR spectrophotometer (Nicolet

Instruments) using a KBr disk. The zeta potential value was measured with a Zeta potential analyzer (Nano Z, Malvern).

The electrochemical experiments were performed with a CHI 660B electrochemical workstation (CH Instruments). The coiled Pt wire and the saturated calomel electrode (SCE) were used as the counter and the reference electrode, respectively. Magnetic stirring was used throughout amperometic measurements to ensure the homogeneity of the solution and the amperometric measurements of choline chloride were performed at the temperature of $37 \pm 1\,^{\circ}C$.

3. Results and discussion

3.1. Characterization

The $FePO_4$ nanostructures were prepared via the reactions between Fe^{3+} and PO_4^{3-} under microwave condition (Yin et al., 2010). In dilute acidic reaction condition, the surface of $FePO_4$ nanostructures is positively charged as verified by the zeta potential measurements, which indicates the value of ζ is about +27.2 mV. Therefore, lattice ion Fe^{3+} ions are abundant on the surface of $FePO_4$ nanostructures, and $Fe(CN)_6^{4-}$ could be adsorbed on the surface of $FePO_4$ for the electrostatic interactions. The adsorbed $Fe(CN)_6^{4-}$ coordinated with the Fe^{3+} on the surface of $FePO_4$ nanostructures and resulted to the formation of PB nanoparticles (Wang and Huang, 2011).

As shown in Fig. 1, before modification, the morphology of $FePO_4$ shows uniform spherical morphology (Fig. 1A), the diameter of $FePO_4$ is about 80 nm. As the PB nanoparticles formed on the surface of $FePO_4$ nanospheres, a significant increase in surface roughness of the $FePO_4$ nanospheres could be observed (Fig. 1B). The attached PB has well distributed on the surface of $FePO_4$, which is expected to be attractive when the PB–$FePO_4$ are used as catalyst for the detection of substrates such as H_2O_2. Because each of the PB nanoparticle is easily and fully accessible to the substrates, turns into an individual electrochemical sensing unit, and thus, yielding a high signal-to-noise ratio (S/N) for the electrochemical determination. Fig. 1C shows the pure PB nanomaterials, as is shown, in the absence of $FePO_4$ nanospheres, PB nanoparticles were apt to accumulate together (Fig. 1C).

3.2. Electrocatalytic oxidation of choline

ChOx was immobilized onto the surface of PB–$FePO_4$. ChOx can catalyze the oxidation of choline to betaine aldehyde, producing H_2O_2 simultaneously, the PB nanoparticles can catalyze the reduction of H_2O_2. Thus, quantification of choline could be achieved by measuring the amount of enzymatically generated H_2O_2. ChOx is negatively charged in pH 8.0 PBS solution because its p*I* is about 4.5 (Qin et al., 2009). PB–$FePO_4$ is also negatively ionized in pH 8.0 PBS solution as evidenced by the measured value of the zeta potential (ca. −17.2 mV). In order to assemble negatively charged ChOx on the surface of PB–$FePO_4$, a positively charged polyelectrolyte, PDDA, was assembled onto the PB–$FePO_4$ layer at first. Owing to the electrostatic force, the negative charge ChOx molecule were directly adsorbed on the positive charge PDDA–PB–$FePO_4$, and ChOx–PDDA–PB–$FePO_4$/GC electrode were fabricated.

The voltammetric responses of the ChOx–PDDA–PB–$FePO_4$/GC electrode in PBS with and without choline chloride are recorded. As shown in part A of Fig. 2, in the absence of choline chloride (curve a), the voltammetric response of the electrode shows a pair of well-defined redox peaks with the anodic (E_{pa}) and cathodic (E_{pc}) peak potential of 0.21 and −0.10 V, respectively, which can be ascribed to the redox reaction of PB (Cao et al., 2010; Qiu et al., 2007; G. Zhao et al., 2005). This indicated that the immobilization of ChOx on the surface of PB–$FePO_4$ does not affect the electrochemical characteristics of PB. Upon addition of 5 mM choline chloride, the shape of the cyclic voltammogram of the electrode changes significantly and characterized by a large cathodic peak at ca. 0.02 V (curve b). The ChOx, catalyzes the oxidation of choline chloride to betaine aldehyde in the presence of oxygen, and producing H_2O_2 simultaneously. Therefore, the cathodic peak at curve b is resulted from the electrocatalytic reduction of the enzymatically generated H_2O_2 at ChOx–PDDA–PB–$FePO_4$/GC electrode. The increase of choline chloride concentration leads to the enhancement of the cathodic current.

To illustrate the special effects of PB–$FePO_4$ toward the oxidation of choline chloride, the CVs of ChOx/GC, ChOx–$FePO_4$/GC and ChOx–PDDA–PB/GC electrode in PBS with and without choline chloride are measured. As shown in part B and C of Fig. 2, the electrocatalytic oxidation of choline chloride can hardly be observed at the ChOx/GC and ChOx–$FePO_4$/GC electrode. The electrocatalytic oxidation of choline chloride at the ChOx–PDDA–PB/GC electrode (part D of Fig. 2) is similar to that of the ChOx–PDDA–PB–$FePO_4$/GC electrode. However, by carefully analyzing the curve b in parts A and D, it is obvious that the onset value for the reduction of enzymatically generated H_2O_2 at the ChOx–PDDA–PB–$FePO_4$/GC electrode occurred at a relatively higher potential (ca. 0.22 V) than it did at the ChOx–PDDA–PB/GC electrode (ca. 0.13 V). Furthermore, the catalytic current at the ChOx–PDDA–PB–$FePO_4$/GC electrode is about 3-fold higher than that at the ChOx–PDDA–PB/GC electrode. These results can be attributed to the better stability of PB–$FePO_4$, the larger surface areas of PB–$FePO_4$ and better dispersibility of PB than that of PB nanomaterials. Therefore, the PB–$FePO_4$ could be a good platform to sensing the oxidase-based substrates.

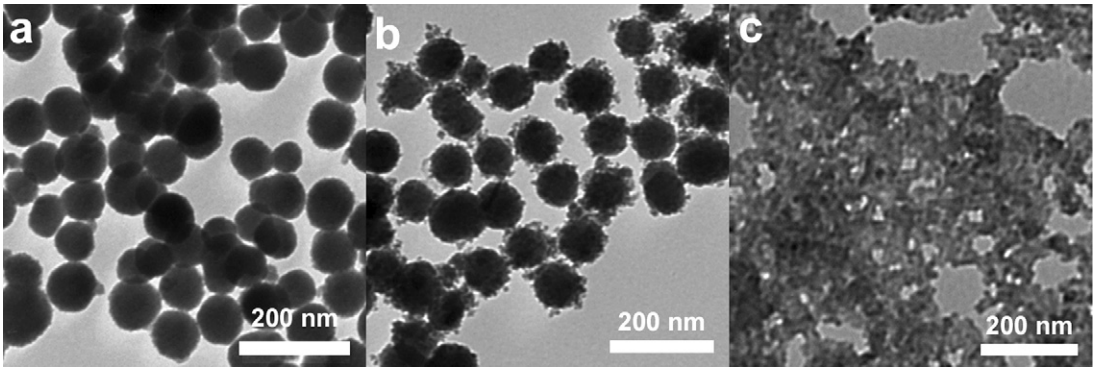

Fig. 1. TEM images of $FePO_4$ (A), PB–$FePO_4$ (B) and PB (C) nanostructures.

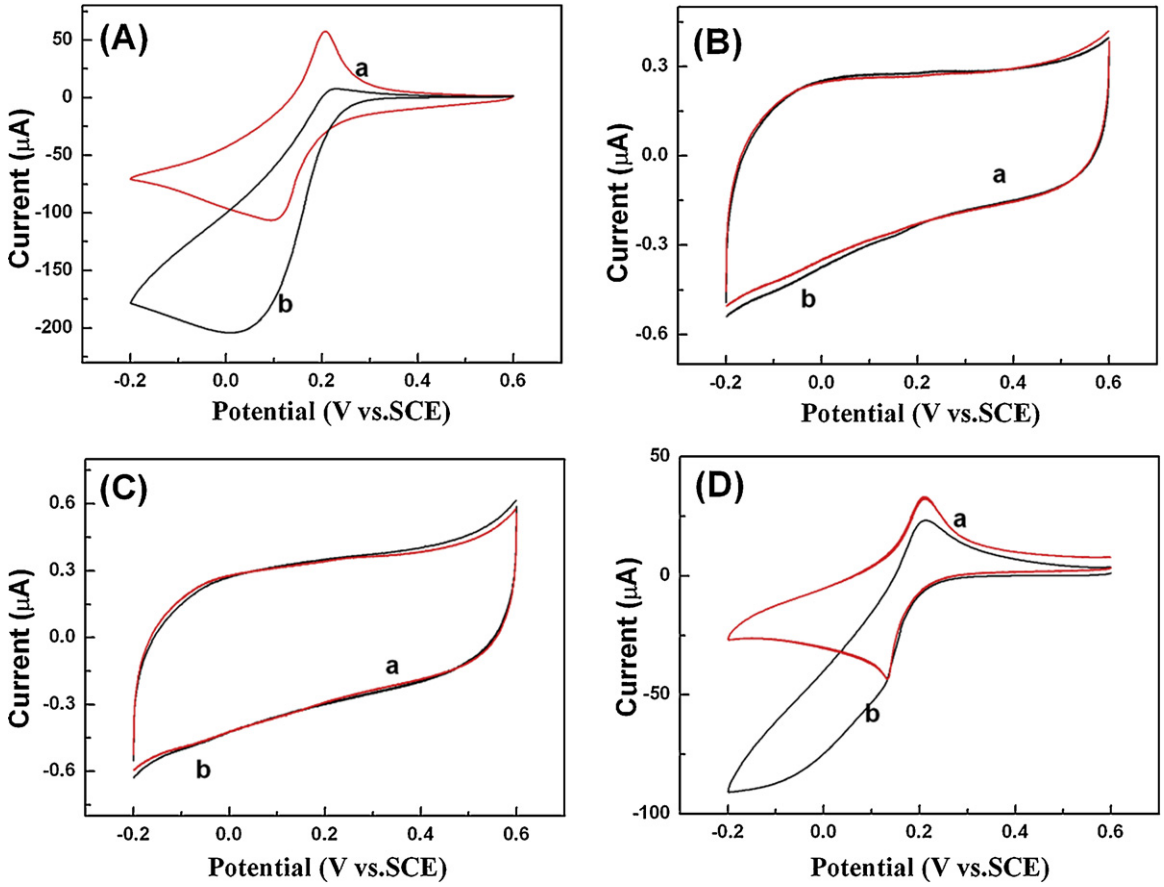

Fig. 2. Cyclic voltammograms of ChOx–PDDA–PB–$FePO_4$/GC (part A), ChOx/GC (part B), ChOx–$FePO_4$/GC (part C) and ChOx–PDDA–PB/GC electrode in the absence (curve a) and presence (curve b) of 5 mM choline chloride in pH 8.0 PBS.

3.3. *Effects of solution pH, temperature, and detection potential*

The response current of the biosensor usually depends on the solution pH, performance temperature, and detection potential. This work optimized these parameters through amperometric measurements. The response current was independently tested thrice for each pH, temperature, and applied potential, and the average value was calculated.

The solution pH has a significant effect on the performance of the biosensor. Within the range of pH 6.0 to 9.0, an optimal response is found at approximately pH 8.0 (panel A of Fig. 3), which is in good agreement with the reported for the native ChOx in solution (Hekmat et al., 2009; Shimomura et al., 2009), and ChOx immobilized on the modified electrode (Dai et al., 2010; Ren et al., 2009; Shimomura et al., 2009). This result indicates that the assembly procedure can keep the native activity of ChOx. In addition, as for the native ChOx in solution, the response decrease more quickly at pH value lower or higher than 8.0 (Shimomura et al., 2009). In this paper, the ChOx–PDDA–PB–$FePO_4$/GC sensor maintained its good response over a broad range of pH values compared to the response of native ChOx in solution. This is due to the good stabilization effect of PDDA–PB–$FePO_4$, and thus prevent the denaturation of enzyme against the change of pH.

The temperature effect of the electrode response was evaluated between 20 and 60 °C. The response increases when the temperature rises from 20 to 30 °C, and then, it reaches a relatively stable value between the temperatures of 30–40 °C (part B of Fig. 3). To a certain extent, the nanomaterials may help to fabricate the microenvironment and retain the bioactivity of enzyme. At a higher temperature, the response decreases might be due to the denaturation of the enzyme. Therefore, the pH 8.0 and temperature 37 °C are chosen as the optimal condition for the ChOx–PDDA–PB–$FePO_4$/GC electrode sensing choline chloride.

The choice of the detection potential is necessary to achieve the lowest detection limit and avoid the electrochemical interfering species. The responses of 0.5 mM choline chloride at different detection potentials were recorded and compared. The results are presented in part C of Fig. 3. Basically, the response keeps on rising when the potential is moved from 0.2 to −0.05 V and decays slightly at −0.1 V. However, a more negative potential leads to the bigger noise. Thus, a detection potential of −0.05 V is selected in this work. Compared with the previous reports, the potential is about 170, 360, 410, 450, and 500 mV more negative than those used at the choline biosensors by immobilizing ChOx at the MWNTs/Pt (Song et al., 2006), MWCNTs–GNp–PDDA/Pt (Qin et al., 2010), HFBI/Au (Zhao et al., 2009), the $\{MWNTs/PANI\}_5/\{PANI\}_3$/GC (Qu et al., 2005), PVA/Au/ChOx/Pt (Ren et al., 2009), and MnO_2/Chit/GC electrode (Bai et al., 2007), respectively (see Table 1).

The low detection potential will significantly diminish the influence of those easily oxidizable species. In real samples, there are some coexisting electroactive species such as glucose, AA, UA, etc., that might affect the biosensor response. The amperometric responses of the ChOx–PDDA–PB–$FePO_4$/GC electrode at the applied potentials of −0.1 to +0.2 with a settled interval of 50 or 100 mV in PBS containing 0.5 mM choline chloride with continuous addition of 0.5 mM AA, 0.5 mM UA and 0.1 mM AP were evaluated, respectively. For a better comparison, at each detection potential, the response current of 0.5 mM choline chloride is set as 100%, and the response of the interfering species is normalized by this value. The results are demonstrated in part D of Fig. 3. When the

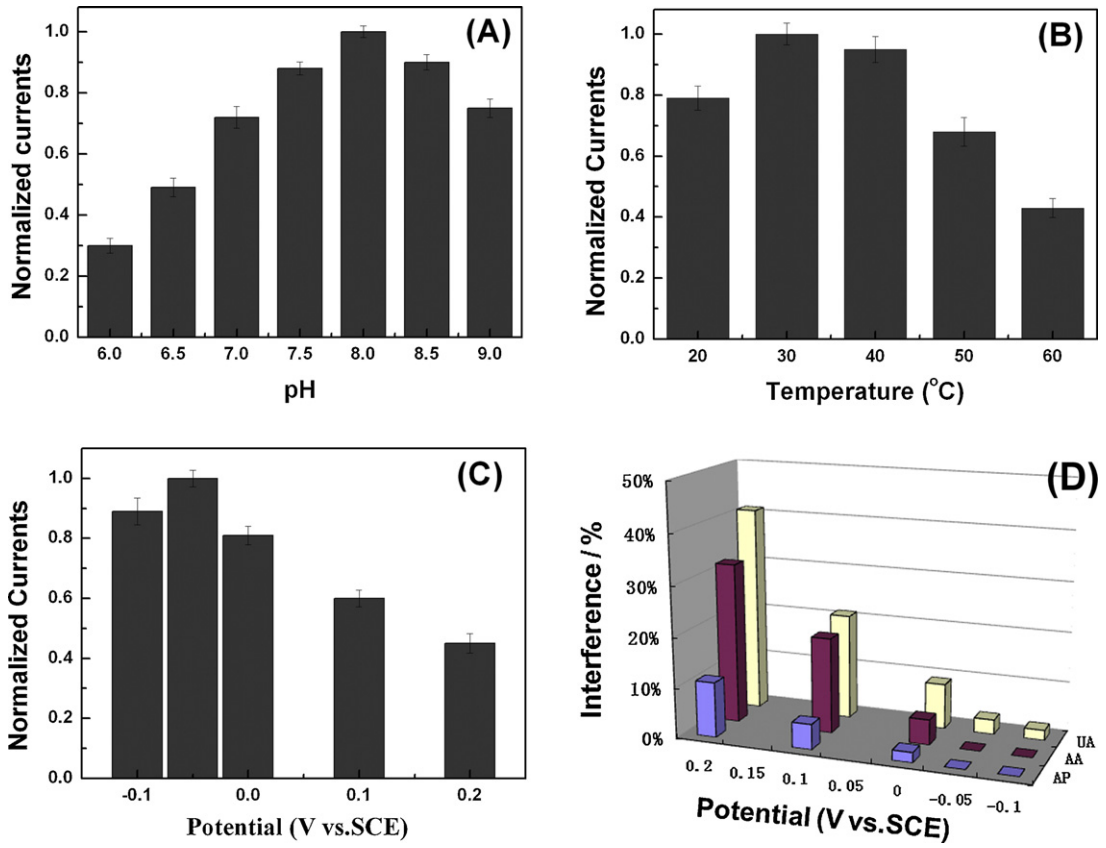

Fig. 3. Dependence of the response of 0.5 mM choline chloride at the ChOx–PDDA–PB–$FePO_4$/GC electrode in PBS (0.1 M) on the pH of the buffer (A), the temperature of the system (B), the detection potential (C) and the selectivity profile of the electrode over interfering agents of UA (0.5 mM), AA (0.5 mM) and AP (0.1 mM) obtained at different applied potentials (D). Every value is an average value of three independent amperometric measurements.

detection potential is more positive than 0 V, the interferences of UA, AA and AP are significant and they increase with the increase of the detection potential. For example, the interferences of UA, AA, and glucose are 21%, 19%, and 5%, respectively, at a potential of 0.1 V, and these values become 41, 32 and 11%, respectively, at a potential of 0.2 V. At the detection potential more negative than −0.05 V, the interferences of AA and AP do not cause any observable interference, and the interference of UA is very small and can be

Table 1
Comparison the detection potential and analytical performance of some ChOx-based choline biosensors.

Choline biosensor	Detection potential (V versus SCE)[a]	Response time (s)	K_M^{app} (mM)	Linear range (mM)	Sensitivity ($\mu A\,mM^{-1}\,cm^{-2}$)	Detection limit (μM)	References
ChOx–PDDA–PB–$FePO_4$/GC	−0.05	2	0.47	0.002–3.2	75.2	0.4 ± 0.05	This work
ChOx–MWNTs/Pt[b]	0.12	8	–	0.005–0.1	–	0.1	Song et al. (2006)
MWCNTs–GNp–ChOx–PDDA/Pt[c]	0.31	7	0.42	0.001–0.5	183.6	0.3	Qin et al. (2010)
ChOx/HFBI/Au[d]	0.36	–	1.30	0.01–1.0	–	–	Zhao et al. (2009)
ChOx–{MWNTs/PANI}$_5$/{PANI}$_3$/GC[e]	0.4	3	–	0.001–2	–	0.3	Qu et al. (2005)
PVA/Au/ChOx/Pt[f]	0.4	20	0.78	0.02–0.4	15.7	10	Ren et al. (2009)
ChOx/MnO_2/Chit/GC[g]	0.45	–	–	0.01–2.1	–	–	Bai et al., 2007
$(ChOx/PDDA)_n/(PVS/PAA)_3$/MWNTs/Pt[h]	0.56	8	–	0.0005–0.1	–	0.7	Qin et al. (2009)
$(ChOx/PDDA)_n/(PVS/PAA)_3$/Pt	0.56	15	–	0.005–0.1	177.4	0.2	Qin et al. (2009)
ChOx–$PVF^+ClO_4^-$/Pt[i]	0.7	–	2.32	Up to 1.2	–	4	Gülce et al. (2003)
ChOx/HRP/CPE[j]	−0.2	15	0.89	0.005–0.6	–	3	Yang et al. (2004)
ChOx–poly(1,2-DAB) nanotubules/PB/Pt[k]	−0.4	10	–	0.05–2	67	50	Curulli et al. (2004)
ChOx–PB/CPE	−0.4	30	1.2	0.02–3	3.5	20	Moscone et al. (2001)

[a] Values of detection potentials versus Ag/AgCl have been adjusted to those versus SCE. This was completed by deducting a constant of 0.04 V to the potential value versus Ag/AgCl.
[b] MWNTs: multi-walled carbon nanotubes.
[c] GNp: gold nanoparticles.
[d] HFBI: hydrophobin.
[e] PANI: polyaniline.
[f] PVA: polyvinyl alcohol.
[g] Chit: chitosan.
[h] PVS: poly(vinyl sulfate); PAA: polyallylamine.
[i] $PVF^+ClO_4^-$: polyvinylferrocenium perchlorate.
[j] CPE: carbon paste electrode.
[k] 1,2-DAB: 1,2-diaminobenzene.

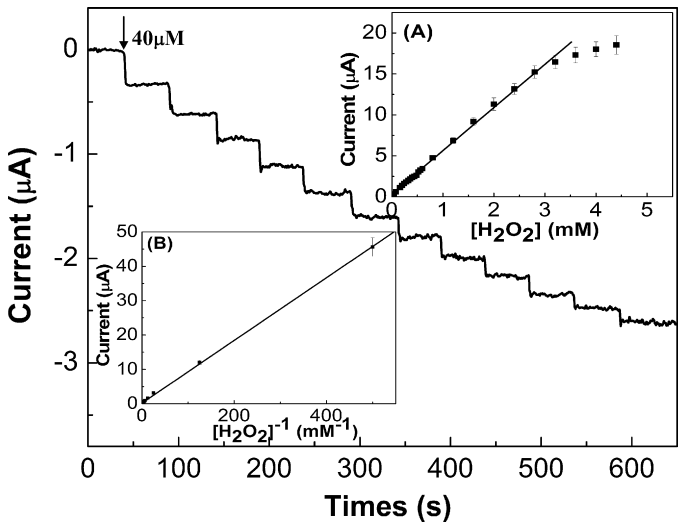

Fig. 4. Amperometric responses of the ChOx–PDDA–PB–$FePO_4$/GC electrode to the successive addition of choline chloride in PBS (0.1 M, pH 8.0) at an applied potential of −0.05 V. The insets show the dependence of the response current of the electrode on choline chloride concentration under the optimal conditions (inset A) and the Lineweaver–Burk plot (inset B).

neglected. By considering the results of part C and D in Fig. 3, the detection potential of −0.05 V is the optimized operating potential.

3.4. Analytical performance of the ChOx–PDDA–PB–$FePO_4$/GC electrode

Fig. 4 shows the typical amperometric response of the ChOx–PDDA–PB–$FePO_4$/GC electrode to the successive addition of choline chloride (40 μM for each addition) in PBS solution at a detection potential of −0.05 V. Immediately after the addition of choline chloride, the response current increases and reaches 95% of the steady-state value within ~2 s. The response time is much shorter than those obtained at other electrodes; for example, the response time is 8 s at ChOx–MWNTs/Pt electrode (Song et al., 2006) and $(ChOx/PDDA)_n/(PVS/PAA)_3$/MWNTs/Pt electrode (Qin et al., 2009), 15 s at $(ChOx/PDDA)_n/(PVS/PAA)_3$/Pt electrode (Qin et al., 2009), and 20 s at PVA/Au/ChOx/Pt electrode (Ren et al., 2009). These results suggest that the ChOx–PDDA–PB–$FePO_4$/GC electrode responds rapidly to the change of the substrate concentration. The electrode linearly responds to choline chloride at lower concentration and reaches saturation level at higher concentration as expected for Michaelis–Menten-type enzyme kinetics. The apparent Michaelis–Menten constant (K_M^{app}) is estimated to be 0.47 mM from the Lineweaver–Burk plot (inset B of Fig. 4), which was lower than the literature value of free ChOx (0.87 mM) (Ohta-Fukuyama et al., 1980), ChOx in the HFBI self-assembled film matrix (1.30 mM) (Zhao et al., 2009) and $PVF^+ClO_4^-$ coated Pt surface (2.32 mM) (Gülce et al., 2003), indicating the good biocompatibility of the PDDA–PB–$FePO_4$ nanostructures. The response current displays a good linear range 2 μM–3.2 mM, with a correlation coefficient of 0.998 and a slope of 5.31 μA mM^{-1}. Therefore, the sensitivity is evaluated to be ~75.2 μA mM^{-1} cm^{-2}. The detection limit is estimated to be ca. 0.4 ± 0.05 μM at a signal-to-noise ratio (S/N) of 3, which is much lower than that obtained at a choline biosensor based on PVA/Au/ChOx/Pt electrode (10 μM) (Ren et al., 2009) and ChOx–PB/CPE (20 μM) (Moscone et al., 2001). The linear response range is wider than those of 5 μM–0.1 mM (Song et al., 2006), 1 μM–0.5 mM (Qin et al., 2010) and 5 μM–0.6 mM (Yang et al., 2004). The sensitivity is also much higher than some of other PB-modified ChOx biosensors (Curulli et al., 2004; Moscone et al., 2001) (the detailed comparison of the analytical characteristics of the developed biosensor with those reported previously is summarized in Table 1). These results suggest that PDDA–PB–$FePO_4$ nanostructures can be used as a good platform for the development of enzyme-based amperometric biosensors for choline determination. It should also point out that ChOx–PDDA–PB–$FePO_4$/GC electrode displays an acceptable repeatability and good stability. The RSD (relative standard deviation) of ~3.2% is estimated from slopes of calibration plots for eight electrodes. The RSD of ~3.1% and ~4.5% is obtained by determinations at the choline chloride concentration of 0.04 mM and 0.4 mM for five times, respectively. In addition, the ChOx–PDDA–PB–$FePO_4$/GC electrode remained 94.6% of its initial current response remained after 2 weeks storage.

4. Conclusions

Electroactive PB–$FePO_4$ nanostructures were prepared by a simple template method. The obtained nanostructures have good electrochemical behavior that can catalyze the reduction of H_2O_2. A new amperometric choline biosensor has been developed by immobilizing ChOx on the PB–$FePO_4$ nanostructures. The biosensor exhibited a fast response, broad linear range, low detection limit with satisfactory stability and repeatability, as well as effective discrimination to the common interfering species. Therefore, the PB–$FePO_4$ nanostructures is a promising candidate in the development of other oxidase-based biosensors.

Acknowledgements

This work is supported by the National Natural Science Foundation of China (20833006, 20905036, and 21175067), Research Fund for the Doctoral Program of Higher Education of China (20103207110004), the Foundation of the Jiangsu Education Committee (09KJA150001, 09KJB150006, 10KJD150007, and 10KJB150009), a Project Funded by the Priority Academic Program Development of Jiangsu Higher Education Institutions, the Foundation of State Key Laboratory Breeding Base of Green Chemistry-Synthesis Technology (GCTKF2010001), the Foundation of Jiangsu Provincial Key Laboratory of Palygorskite Science and Applied Technology (HPK201102 and HPK201005), and the Eleventh Five-year Research Program of Jiangsu Institute of Education (JSjy2008qz03).

Appendix A. Supplementary data

Supplementary data associated with this article can be found, in the online version, at doi:10.1016/j.bios.2011.10.026.

References

Bai, Y.H., Du, Y., Xu, J.J., Chen, H.Y., 2007. Electrochem. Commun. 9, 2611–2616.
Bai, Y.H., Zhang, H., Xu, J.J., Chen, H.Y., 2008. J. Phys. Chem. C 112, 18984–18990.
Campanella, L., Mascini, M., Palleschi, G., Tomassetti, M., 1985. Clin. Chim. Acta 151, 71–83.
Campanella, L., Tomassetti, M., De Angelis, G., Sammartino, M.P., Cordatore, M., 1987. Clin. Chim. Acta 169, 175–182.
Cao, L.Y., Liu, Y.L., Zhang, B.H., Lu, L.H., 2010. ACS Appl. Mater. Interfaces 2, 2339–2346.
Carter, N., Trenerry, V.C., 1996. Electrophoresis 17, 1622–1626.
Curulli, A., Valentini, F., Orlanduci, S., Terranova, M.L., Palleschi, G., 2004. Biosens. Bioelectron. 20, 1223–1232.
Dai, H., Chi, Y.W., Wu, X.P., Wang, Y.M., Wei, M.D., Chen, G.N., 2010. Biosens. Bioelectron. 25, 1414–1419.
Ding, Y., Gu, G., Xia, X.H., 2008. J. Solid State Electrochem. 12, 553–558.
Fleming, J.K., Gadsden, R.H., 1987. Clin. Biochem. 20, 249–256.
Gülce, H., Akta, Y.S., Gülce, A., Yıldız, A., 2003. Enzyme Microb. Technol. 32, 895–899.
Hekmat, A., Saboury, A.A., Divsalar, A., 2009. Biophys. J. 96, 582a.
Ikarashi, Y., Maruyama, Y., 1993. J. Chromatogr. B 616, 323–326.
Jenny, A., Ashok, K., Reinhard, S., 2002. Brain Res. 953, 17–30.
Karyakin, A.A., Karyakina, E.E., Gorton, L., 2000. Anal. Chem. 72, 1720–1723.
Karyakin, A.A., Kotel'nikova, E.A., Lukachova, L.V., Karyakin, E.E., Wang, J., 2002. Anal. Chem. 74, 1597–1603.

Karyakin, A.A., Puganova, E.A., Budashov, I.A., Kurochkin, I.N., Karyakina, E.E., Levchenko, V.A., Matveyenko, V.N., Varfolomeyev, S.D., 2004. Anal. Chem. 76, 474–478.
Katz, E., Willner, I., 2004. Angew. Chem.-Int. Ed. 43, 6042–6108.
Mamoru, A., 2003. Catal. Today 85, 193–198.
Margrit, K., Jenny, A., Ashok, K., Dietlind, S., Osama, S., Jörg, S., Matthias, S., Reinhard, S., 2003. Int. J. Dev. Neurosci. 21, 357–369.
Moscone, D., D'Ottavi, D., Compagnone, D., Palleschi, G., Amine, A., 2001. Anal. Chem. 73, 2529–2535.
Ohta-Fukuyama, M., Miyake, Y., Emi, S., Yamano, T., 1980. J. Biochem. 88, 197–203.
Okawa, H., Yabuki, J., Kawamura, Y., Arise, I., Sato, M., 2008. Mater. Res. Bull. 43, 1203–1208.
Qu, F.L., Yang, M.H., Jiang, J.H., Shen, G.L., Yu, R.Q., 2005. Anal. Biochem. 344, 108–114.
Qin, X., Wang, H.C., Wang, X.S., Li, S., Miao, Z.Y., Huang, N., Chen, Q., 2009. Mater. Sci. Eng. C 29, 1453–1457.
Qin, X., Wang, H.C., Wang, X.S., Miao, Z.Y., Chen, L.L., Zhao, W., Shan, M.M., Chen, Q., 2010. Sens. Actuators B: Chem. 147, 593–598.
Qiu, J.D., Peng, H.Z., Liang, R.P., Li, J., Xia, X.H., 2007. Langmuir 23, 2133–2137.
Qiu, J.D., Xiong, M., Liang, R.P., Zhang, J., Xia, X.H., 2008. J. Nanosci. Nanotechnol. 8, 4453–4460.
Ramana, C.V., Mauger, A., Gendron, F., Julien, C.M., Zaghib, K., 2009. J. Power Sources 187, 555–564.
Razola, S.S., Pochet, S., Grosfils, K., Kauffmann, J.M., 2003. Biosens. Bioelectron. 18, 185–191.
Ren, T., Yan, L., Zhang, X.M., Suo, J.S., 2003. Appl. Catal. A 244, 11–17.
Ren, X.L., Tang, F.Q., Liao, R., Zhang, L., 2009. Electrochim. Acta 54, 7248–7253.
Rinne, J.O., Myllykyla, T., Lonnberg, P., Marjamaki, P., 1991. Brain Res. 547, 167–170.
Sanz-Vicente, I., Romero, J.J., de Marcos, S., Ostra, M., Ubide, C., Galbán, J., 2009. J. Fluoresc. 19, 583–591.
Shi, H.B., Yang, Y., Huang, J.D., Zhao, Z.X., Xu, X.H., Anzai, J., Osa, T., Chen, Q., 2006. Talanta 70, 852–858.
Shimomura, T., Itoh, T., Sumiya, T., Mizukami, F., Ono, M., 2009. Talanta 78, 217–220.
Song, Z., Huang, J.D., Wu, B.Y., Shi, H.B., Anzai, J.I., Chen, Q., 2006. Sens. Actuators B: Chem. 115, 626–633.
Wang, H., Huang, Y.M., 2011. J. Hazard. Mater. 191, 163–169.
Wang, J., Liu, G.D., Lin, Y.H., 2006. Analyst 131, 477–483.
Yang, M.H., Yang, Y.H., Yang, Y., Shen, G.L., Yu, R.Q., 2004. Anal. Biochem. 334, 127–134.
Yin, Y.J., Zhang, H., Wu, P., Zhou, B., Cai, C.X., 2010. Nanotechnology 21, 425504.
Zhang, L., Liu, Y.H., Chen, G.N., 2004. J. Chromatogr. A 1043, 317–321.
Zhang, Z.X., Wang, J., Wang, X.L., Wang, Y., Yang, X.R., 2010. Talanta 82, 483–487.
Zhao, G., Feng, J.J., Zhang, Q.L., Li, S.P., Chen, H.Y., 2005. Chem. Mater. 17, 3154–3159.
Zhao, W., Xu, J.J., Shi, C.G., Chen, H.Y., 2005. Langmuir 21, 9630–9634.
Zhao, Z.X., Wang, H.C., Qin, X., Wang, X.S., Qiao, M.Q., Anzai, J.I., Chen, Q., 2009. Colloid Surf. B 71, 102–106.